Research Article

Synthesis and Properties of Red Mud-Based Nanoferrite Clinker

Hongfang Sun [iD],[1] **Chuyu Chen,**[1] **Li Ling,**[1] **Shazim Ali Memon** [iD],[2] **Zhu Ding,**[1] **Weiwen Li** [iD],[1] **Lu-ping Tang,**[3] **and Feng Xing** [iD][1]

[1]*Guangdong Provincial Key Laboratory of Durability for Marine Civil Engineering, College of Civil and Transportation Engineering, Shenzhen University, Shenzhen 518060, China*
[2]*Department of Civil Engineering, Nazarbayev University, Astana 010000, Kazakhstan*
[3]*Division of Building Technology, Chalmers University of Technology, Gothenburg 41296, Sweden*

Correspondence should be addressed to Feng Xing; xingf@szu.edu.cn

Red mud, an industrial waste obtained from alumina plants, is usually discharged into marine or disposed into a landfill polluting the surrounding water, atmosphere, and soil. Thus, disposal of red mud is an environmental concern and it should be recycled in an effective way. Since red mud consists of iron- and aluminum-rich phases, it can potentially be processed into cementitious material and can be used for a construction purpose. This research investigated the synthesis of nanoferrite (NF) clinker by using red mud as a raw material through chemical combustion technology for potential use in cement-based composite. Before the synthesis of NF, red mud was characterized by using XRF, XRD, and SEM techniques. From characterization results, the stoichiometric ratio of raw materials was calculated and experimentally optimized. The sample was then tested at various temperatures (815, 900, 1000, and 1100°C) to find the optimum synthesis temperature. Finally, the hydraulic activity of NF was verified and the contribution to mechanical properties was determined by replacing cement with NF at various substitution levels (0, 5, 10, and 20 wt%). Test results showed that the optimum condition for the synthesis of NF was found when the ratio of $CaCO_3$/red mud was 1.5 and the sintering temperature was 815°C. The synthesized NF had an average diameter of 300 nm, and the main composition was brownmillerite (C_4AF) with distinct hydraulic reaction. When NF was used as a substitute of Portland cement in mortar, the flexural strength with a 5% replacement level improved by 15%. Therefore, it can be concluded that the synthesis of NF provides an alternative approach to recycle red mud and could significantly help in reducing environmental pollution.

1. Introduction

Red mud, produced by the Bayer process, is an industrial waste obtained during the production of aluminum. For every ton of alumina produced, approximately 1.6 tons of red mud is released and it is estimated that more than 66 million tons of this waste is annually generated worldwide [1, 2]. The red mud is usually discharged into marine [3] or disposed into land [4] polluting the surrounding water, atmosphere, and soil, especially in the areas where this industry is located [5]. Therefore, steps must be taken to recycle this waste in an eco-friendly way.

Based on the composition of red mud, it can be recycled and used in a variety of fields. For example, it can be used as a recovery of metals or can be used as a potential alternative catalyst since it mainly consists of a mixture of oxides of Fe, Al, and Ti and a smaller amount of Si, Ca, and Na [6, 7]. Red mud can also act as a pigment since its iron-rich phases have a red color [8]. However, a large amount of red mud still needs to be recycled and more effective applications should be developed. Recently, the application of red mud as building materials has attracted the research community [9]. Calcined red mud usually consists of elements Si, Al, and Fe and has shown pozzolanic reactivity [10]. Thus, it has a potential to be used as a cementitious material. Till to date, a variety of red mud-based cements have been fabricated, such as Portland cement [11], self-compacting cement [12], and alkali-activated cement [13]. However, it could greatly enlarge the

application area of red mud if new cement-based composites containing red mud are developed.

Ferrite cement has a variety of excellent properties such as high strength, impermeability, antifreeze, and corrosion resistance. Consequently, it can be used for various applications, such as emergency repair, winter construction, antiseepage, plugging, underground foundation, and high-strength concrete production [14]. However, the hydration rate of ferrite cement is slow (several years or even decades to fully hydrate) [15], which greatly limits its popularity. One of the effective approaches to accelerate the early hydration is to reduce the particle size of ferrite cement [16], especially down to nanoscale [17–20]. The most commonly used technique to reduce the particle size of ferrite cement is grinding, which consumes a lot of energy. The ground particles usually have a wide particle size distribution with an irregular shape which might not be conducive to the workability of concrete. Furthermore, it is an uphill task to reduce the particle size to a nanometer scale [21]. Therefore, it is necessary to develop an effective and economical way to refine the particle size of ferrite cement.

In this research, iron-rich red mud was used to synthesize nanoferrite (NF) clinker through a chemical combustion method at a much lower temperature ($\leqq 1150°C$) than traditional ferrite cement (1250-1300°C). The production conditions were theoretically designed and experimentally optimized. After optimization, the hydration activity and mechanical properties of NF admixture were determined.

2. Materials and Methods

2.1. Materials. Red mud and limestone were used as raw materials while urea and nitric acid were used as a fuel to produce NF. Red mud is an industrial waste produced by the Bayer process. The purity of $CaCO_3$ in limestone and H_2NCOCH_2 in urea were greater than 95.5% and 99%, respectively, while the content of HNO_3 in concentrated nitric acid was 65-68%. The raw material (limestone), urea, and concentrated nitric acid were purchased from Xilong Scientific Co. Ltd. (Guangzhou, China). In order to investigate the hydration and mechanical properties of NF, P·I type ordinary Portland cement (OPC) produced by China United Cement Qufu Co. Ltd. (Qufu, China) and having the following composition (Table 1) was used.

2.2. Synthesis of NF. The production procedure of NF is as follows: Firstly, raw materials (red mud and limestone) and fuel (urea and nitric acid) were mixed and placed in a muffle furnace. The heating temperatures of the samples in the muffle furnace were set at 815, 900, 1000, and 1100°C, respectively. The temperature of the samples was raised from room temperature to the set temperature (815, 900, 1000, and 1100°C) and held for 15 minutes. Then, the samples were rapidly taken out and allowed to cool in the air. Finally, the cooled samples were ground to obtain the final NF powder. The mass ratios of red mud to $CaCO_3$ in the raw materials were 1 : 0.5, 1 : 0.6, 1 : 0.7, 1 : 0.8, 1 : 0.9, 1 : 1, and 1 : 2 while the raw materials-to-fuel ratio was 0.24 : 1. The role of the fuel was to provide the raw materials with the heat required

TABLE 1: Composition of Portland cement (%).

SiO$_2$	Al$_2$O$_3$	Fe$_2$O$_3$	CaO	MgO	SO$_3$
22.12	4.51	3.45	64.92	3.35	0.4

for reaction so as to lower the sintering temperature and to refine the product. The mass ratio of urea to nitric acid in fuel was 2.02 : 1.

2.3. Testing

2.3.1. Scanning Electron Microscopy (SEM). In this research, the secondary electron (SE), backscattered electron (BSE), and energy dispersive X-ray spectroscopy (EDS) in SEM were used to evaluate the morphology and composition of red mud and NF before and after hydration. The SEM observation was performed on FEI Quanta 250 (FEI Inc., Hillsboro, OR, USA) with a field emission gun and an accelerating voltage of 15 kV. The SE images provide the information on the morphology of the surface while BSE images combined with EDS mapping provide the cross-sectional microstructure and information about the chemistry of the analyzed samples.

The unhydrated and hydrated NF were observed directly by the SE technique. For BSE, the raw red mud powder and unhydated NF were prepared by adopting the following procedure. At first, mix the same mass of red mud and epoxy resin (containing a curing agent) to form viscous slurry. The slurry was poured into a cylindrical mold (10 mm diameter and 55 mm height) and cured at room temperature for 24 hours. The solidified sample was then cut by a low-speed diamond saw to expose the fresh surface. Thereafter, the surface was polished using diamond pastes of gradations 9, 6, 3, 1, and 0.25 μm on top of Texmet papers.

In order to observe hydrated NF samples through BSE, the following procedure was adopted. Take the weight of NF powder and deionized water in a mass ratio of 1.0, and mix for 2 minutes. The mixture was poured into a mold ($10 \times 10 \times 10$ mm^3), consolidated, and cured at room temperature ($20 \pm 2°C$). After curing for 3, 7, 14, 28, and 56 days, the samples were taken out for testing (only the 28-day sample was used for SEM observation while samples cured at other ages as well as 28 days were used for XRD examination). The 28-day samples were then cut into 2 cm thick pieces and vacuum-saturated with epoxy for 24 h at room temperature. Thereafter, the specimens were cut with a slow speed diamond saw to expose a fresh surface by following the procedure as mentioned in the previous paragraph. Before loading the specimen into the SEM chamber, the specimens were sputter coated using gold to form a conductive surface.

2.3.2. X-Ray Diffraction (XRD). To obtain the mineralogical composition of red mud powder and NF before and after hydration, XRD was performed on a Bruker D8 instrument (Bruker, Karlsruhe, Germany) using a CuKα X-radiation ($\lambda = 1.5406$ Å) at 40 kV and 40 mA while Jade program 6.5 was used for quantitative analysis.

2.3.3. X-Ray Fluorescence (XRF). The elemental composition of red mud powder was evaluated using a Bruker S4 Explorer

XRF instrument (Bruker AXS, Germany) equipped with an X-ray tube with an operating voltage of 50 kV and a current of 50 mA. The exit spot at the end of the beamline was adjusted by the slit to $50 \times 60 \, \mu m^2$. The sample was kept 1 m away from the slit at a 45° angle to the X-ray beam, while the detector was 3-10 cm away at an angle of 45° with the sample. The effective exposure time of each sample in the experiment was 600 s.

2.3.4. BET Surface Area. The specific surface area of unhydrated NF powder was tested by a BET instrument in a fully automated TriStar II Surface Area and Porosity Analyzer from Micromeritics Instrument Corporation. Before the experiment, each sample was degassed in a vacuum at 105°C for more than 6 hours. In this experiment, nitrogen was used as the adsorption gas.

2.3.5. Mechanical Properties. In order to evaluate the mechanical properties of NF material, the compressive and flexural strength tests were conducted. For these tests, cement mortar samples having a size of $10 \times 10 \times 40 \, mm^3$ were prepared with NF at different levels of cement substitution (0, 5, 10, 15, and 20 wt% replacement of OPC by NF). The water-to-binder ratio and the binder-to-sand ratio used were kept as 0.35 and 1, respectively, while the dosage of the superplasticizer was 0.55%. In order to reduce the influence of large sand particle size on the test specimens, the sand having a size of more than 1 mm was removed by sieving. A YZH-300 testing machine (Luda Machinery Instrument Co. Ltd., Zhejiang, China) was used to determine the mechanical properties at the age of 3, 7, 14, and 28 days. The strength value represented the average of three specimens.

3. Results and Discussion

3.1. Synthesis of NF

3.1.1. Characterization of Red Mud Raw Material. During the synthesis of NF, red mud acted as an iron and aluminum source while limestone acted as a calcium source. They reacted with the assistance of heat provided by both furnace and fuel (urea and nitric acid). It is known that the composition and characterization of limestone and fuel (urea and nitric acid) are simple, and the only factor that needs to be considered is the purity of the samples. However, the characterization of red mud raw material, which is a complex mixture of more than ten kinds of compounds, is not an easy task. The precise characterization of red mud is an important step before its applications are considered. According to the available literature [22], most of the time, red mud is usually characterized by only XRD or XRF methods. However, XRD spectrum of the red mud sample is difficult to analyze due to the presence of multiphases in red mud, which leads to overlapping peaks. As far as XRF is concerned, it can only identify the relative proportion of elements instead of phases, although it is important for the stoichiometric calculation. Therefore, in order to accurately characterize the composition of red mud, firstly, an element mapping technique (EDS combined with BSE in SEM) was used to narrow down

the range of elements. Then, phase identification and quantitative analysis were performed by the XRD. Finally, for a verification purpose, the results were compared with XRF.

Figure 1 presents a typical BSE image and corresponding element mapping results of red mud. It is clear that red mud powder contains a large amount of Fe and Al elements as well as some Na, Si, Ca, and O. The mapping results of elements H and C are not shown here since it is believed that part of them came from epoxy resin and was introduced during a sample preparation process. Moreover, element H was also beyond the detection limit of this technique. However, actually, they might possibly exist in red mud. Therefore, it was speculated that elements with possible positive valency were C, Si, H, and the aforementioned metals, while the element with negative valence was O. Therefore, red mud might contain components possibly having Al-Si-Na-O (-H and/or -C), Al-O (-H and/or -C), Fe-O (-H and/or -C), and Ca-O (-H and/or -C). It is suggested that Ti-O (-H and/or -C) and Fe-Ti-O (-H and/or -C) might also have formed. Based on the above analysis, the XRD spectrum was obtained and analyzed to further characterize the composition of red mud.

Based on the elemental range as shown in Figure 1, the phase identification and quantitative analysis of red mud were performed through XRD and the results are presented in Figure 2 and Table 2. It can be seen that Fe-related phases in red mud are in the forms of Fe_2O_3 (33.4%), Fe_3O_4 (1.4%), and FeOOH (2.8%, decomposition temperature of 400°C) [23]. The Al-related phases consist of AlO(OH) (10.7%, decomposition temperature of 430°C) [24], $Na_{7.88}(Al_6Si_6O_{24})(CO_3)_{0.93}$ (6.8%, decomposition temperature of 520°C) [25], Al_2TiO_5 (3.4%, decomposition temperature of 800°C) [26], and $Na_{0.33}Ca_{0.67}Al_{11.67}Si_{2.33}O_8$ (1.3%, decomposition temperature of 800°C) [27]. Moreover, a small amount of Ca-related phases was detected in the forms of $CaCO_3$ (5.0%) and $Na_{0.33}Ca_{0.67}Al_{11.67}Si_{2.33}O_8$ (1.3%). Minor SiO_2 (6.4%) and TiO_2 (4.5%) were also found. Based on the above analysis, it can be seen that all Al-related phases $Na_{7.88}(Al_6Si_6O_{24})(CO_3)_{0.93}$, $Na_{0.33}Ca_{0.67}Al_{1.67}Si_{2.33}O_8$, and Al_2TiO required extra heat to synthesize NF. As far as Fe-related phases are concerned, FeOOH required extra heat to synthesize NF while the other forms of Fe (Fe_2O_3 and Fe_3O_4) can directly be used to form NF. Therefore, decomposition temperature of both Fe- and Al-related phases was above 800°C and was set to be the minimal temperature required for sintering NF. It should also be noticed that SiO_2 and CaO components obtained from either red mud or decomposition reaction (such as decomposition of $CaCO_3$ at 900°C) may also produce belite with hydraulic activity.

In order to verify the XRD results presented in Table 2, the composition of red mud was converted to oxide composition and compared with XRF results as shown in Table 3. The comparison indicates that the XRD and XRF results are in good agreement with percentage errors in most cases within 10%. Despite Na_2O having an error of 23.5%, the difference between the content determined by XRF (11.7%) and XRD (8.95%) is acceptable. This mutual verification confirmed the accuracy of the composition of analyzed

(a) BSE

(b) Fe

(c) Al

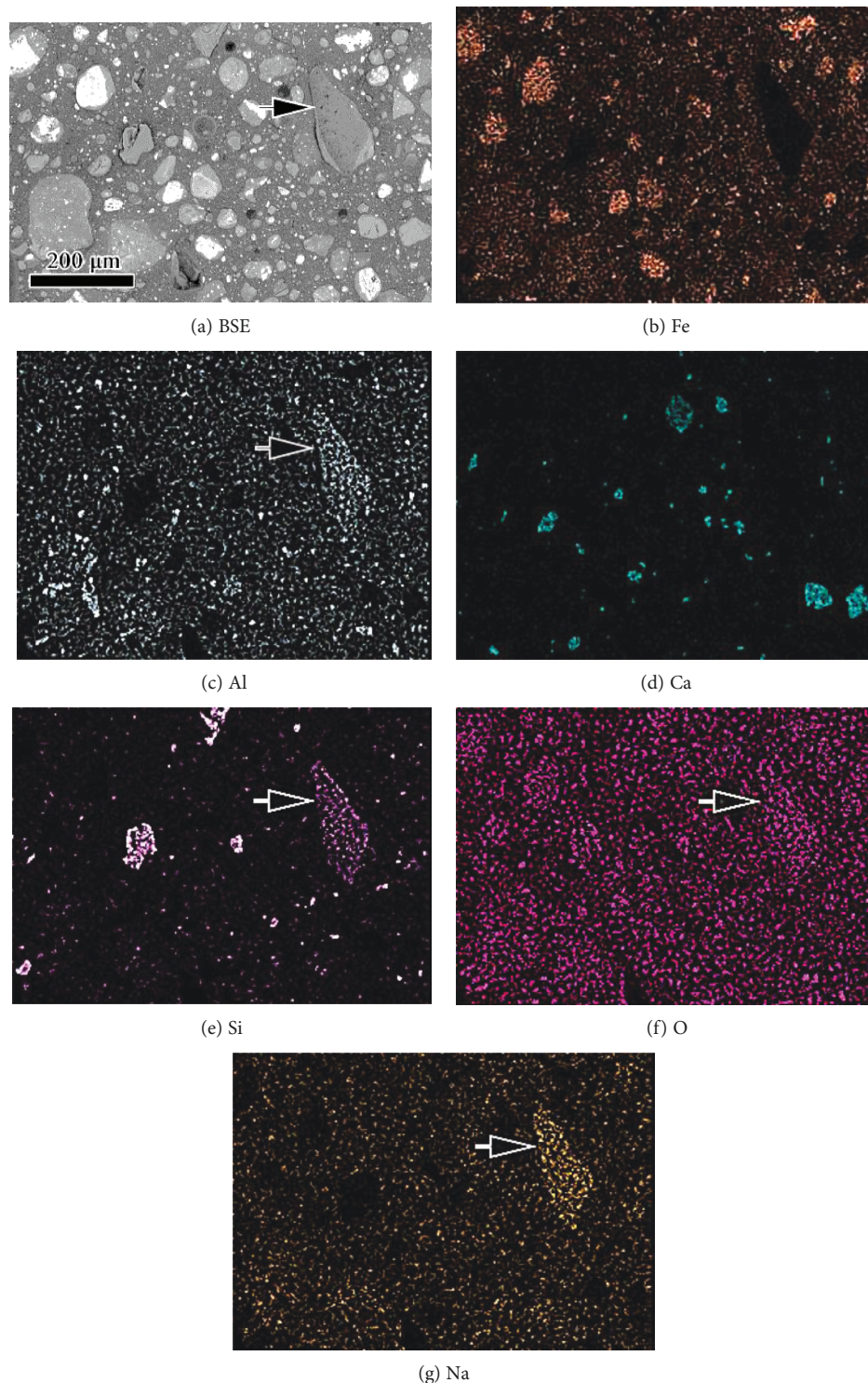(d) Ca

(e) Si

(f) O

(g) Na

Figure 1: BSE and element mapping results of red mud powder. The arrows indicate particles simultaneously containing elements Na, Al, Si, and O.

red mud raw material, which forms foundation for the synthesis of NF.

3.1.2. Stoichiometric Calculation of NF Synthesis with Red Mud. In order to experimentally synthesize NF, stoichiometric calculation of raw materials was performed.

According to the composition of NF (target compound was Ca_2FeAlO_5, abbreviated to C_4AF) [28], the raw materials are required to consist of oxides of CaO, Fe_2O_3, and Al_2O_3, part of which can be provided by red mud while the remaining has to be provided by supplementary materials.
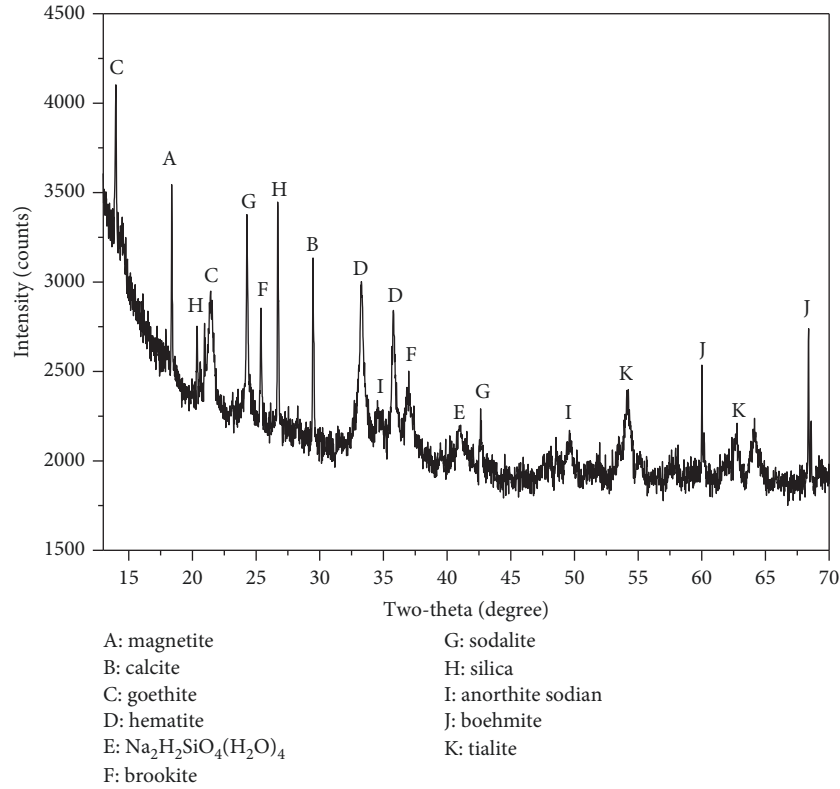
FIGURE 2: XRD spectrum of red mud.

A: magnetite
B: calcite
C: goethite
D: hematite
E: $Na_2H_2SiO_4(H_2O)_4$
F: brookite

G: sodalite
H: silica
I: anorthite sodian
J: boehmite
K: tialite

TABLE 2: Composition of red mud from quantitative XRD analysis.

Compositions of red mud	Content (%)
Silica (SiO_2)	6.4
Sodalite ($Na_{7.88}(Al_6Si_6O_{24})(CO_3)_{0.93}$)	6.8
Sodium dihydrogen silicate tetrahydrate ($Na_2H_2SiO_4(H_2O)_4$)	24.3
Anorthite sodian ($Na_{0.33}Ca_{0.67}Al_{1.67}Si_{2.33}O_8$)	1.3
Calcite ($CaCO_3$)	5.0
Magnetite (Fe_3O_4)	1.4
Hematite (Fe_2O_3)	33.4
Boehmite ($AlO(OH)$)	10.7
Goethite ($FeOOH$)	2.8
Brookite (TiO_2)	4.5
Tialite (Al_2TiO_5)	3.4

TABLE 3: Comparison between XRD and XRF results of red mud.

Oxide	Fe_2O_3	Al_2O_3	SiO_2	Na_2O	TiO_2	CaO
XRF result (%)	37.69	24.4	16.8	11.7	5.33	2.83
XRD result (%)	37.38	22.36	16.23	8.95	5.99	2.80
Deviation (%)	0.82	8.36	3.39	23.50	12.4	1.06

Assuming that CaO, Fe_2O_3, and Al_2O_3 are decomposed completely from red mud during the synthesis of NF [29], according to the following formula [30]:

$$4CaO + Fe_2O_3 + Al_2O_3 \longrightarrow 4CaO \cdot Fe_2O_3 \cdot Al_2O_3, \quad (1)$$
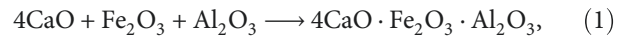
it can be seen that theoretically in 100 g of red mud, maximum 37.38 g of Fe_2O_3 and 52.33 g of CaO can be used to produce C_4AF with the assistance of 25.23 g of Al_2O_3. By looking at the oxide composition of red mud in Table 3, it seems that extra Fe_2O_3 exists in red mud while the quantity of CaO (2.83 g) required is far from enough. However, it should be noticed that during sintering, SiO_2 may consume CaO to generate silicate. Thus, more calcium source should be added so that it can possibly react with both Fe_2O_3 and SiO_2. It is worth noting that at the synthesis temperature of C_4AF (1000-1100°C) [31], it is possible to generate hydraulic C_2S, which does not have a negative effect on C_4AF. The production of C_2S is based on the following formula:

$$2CaO + SiO_2 \longrightarrow 2CaO \cdot SiO_2. \quad (2)$$
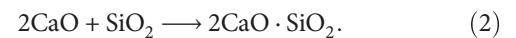
It can be seen that in 100 g red mud, stoichiometrically, 16.80 g SiO_2 reacts with 31.36 g CaO to synthesize C_2S. Therefore, in total, 81.30 g of extra CaO is required to form C_4AF and C_2S, corresponding to 145.18 g of $CaCO_3$. In other words, the mass ratio of $CaCO_3$ added to red mud is about 1.5, and at this mass ratio, theoretically, 114.4 g of C_4AF and 48.16 g of C_2S can be generated.
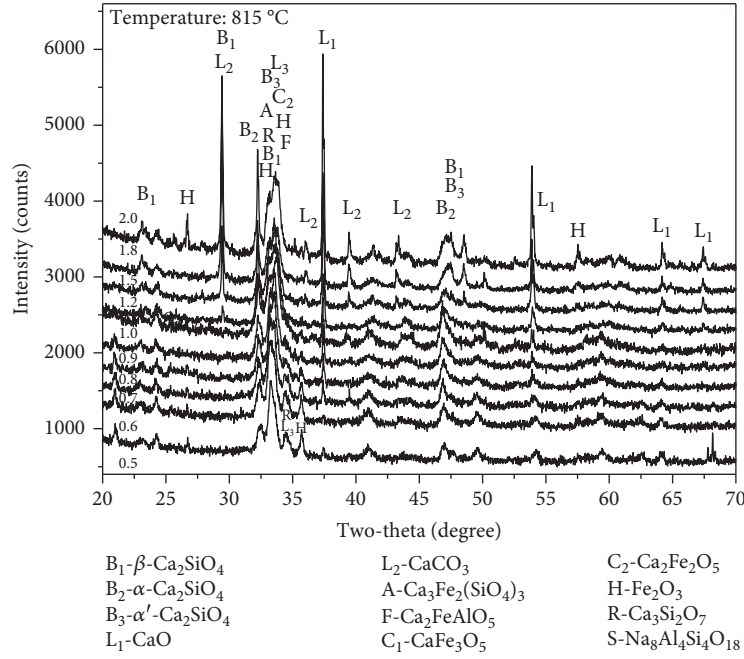
FIGURE 3: XRD spectra of NF produced at different $CaCO_3$/red mud ratios.

TABLE 4: Variation in content of major phases in NF at different $CaCO_3$/red mud ratios (%).

$CaCO_3$/red mud (wt%)	0.5	0.6	0.7	0.8	0.9	1.0	1.2	1.5	1.8	2.0
Ca_2FeAlO_5 (brownmillerite)	**19.2**	**21.7**	**23.4**	**32.1**	**39.0**	**36.3**	**41.5**	**47.2**	**39.8**	**34.9**
$Ca_2Fe_2O_5$ (srebrodolskite)	14.1	22.5	26.1	30.9	18.0	19.2	13.3	10.4	10.3	9.0
$CaFe_3O_5$ (calcium iron oxide)	6.4	4.3	4.4	3.7	3.9	4.4	5.4	2.8	2.5	3.7
$Ca_3Fe_2(SiO_4)_3$ (andradite)	2.1	3.5	2.7	0.6	2.6	2.7	0.6	1.7	0.3	2.1
Fe_2O_3 (hematite)	14.8	17.2	12.8	9.4	5.5	3.3	5.0	2.5	2.3	3.4
β-Ca_2SiO_4 (dicalcium silicate)	14.0	9.5	6.3	5.2	7.0	7.5	6.9	7.4	7.2	6.2
α-Ca_2SiO_4 (dicalcium silicate)	2.3	3.5	3.9	4.2	6.1	0.5	0.8	0.9	0.7	0.6
α'-Ca_2SiO_4 (dicalcium silicate)	1.5	0.2	0.2	0.1	0.2	1.4	0.2	0.3	0.2	0.2
Ca_2SiO_4 (sum(α+α'+β)) (dicalcium silicate)	**17.8**	**13.2**	**10.4**	**9.5**	**13.3**	**9.4**	**8.0**	**8.6**	**8.1**	**7.0**
$Ca_3Si_2O_7$ (rankinite)	12.9	12.5	12.8	8.3	11.5	16.8	15.8	10.5	11.0	8.2
$CaCO_3$ (calcite)	0.6	0.1	0.1	0.1	0.1	2.2	2.5	6.2	15.1	16.2
CaO (lime)	1.6	1.1	2.8	3.4	3.9	3.2	7.0	8.8	9.8	13.8
$(CaO)_{12}(Al_2O_3)_7$ (mayenite)	0	0	0.5	0.1	0.3	1.2	0.4	0.6	0.1	0
$NaAlSi_4$ (sodium aluminium silicon)	1.2	1.8	1.7	1.0	1.7	3.2	0.6	0.7	0.7	1.7
$Na_8Al_4Si_4O_{18}$ (sodium aluminum silicate)	9.7	1.8	2.3	0.9	0.3	0	0	0	0	0

In order to verify the above theoretical analysis, the ratios of $CaCO_3$/red mud were experimentally adjusted to around 1.5 as 0.5, 0.6, 0.7, 0.8, 0.9, 1.0, 1.2, 1.5, 1.8, and 2.0, respectively, and optimized. Since the heating temperature might also influence the final composition of NF, the influence of various temperatures (815, 900, 1000, and 1100°C) was also investigated.

3.1.3. Influence of $CaCO_3$/Red Mud Raw Materials. The raw materials and the fuel were mixed to synthesize NF. The influence of $CaCO_3$/red mud on NF composition is shown

in Figure 3 and Table 4, respectively, while the change in the content of main phases in NF with varying $CaCO_3$/red mud ratios is shown in Figure 4. It can be seen that with the increase in the ratio of $CaCO_3$/red mud from 0.5 to 2.0, the content of the target product Ca_2FeAlO_5 (brownmillerite, C_4AF) firstly increased and then decreased. The peak value of 47.2% was achieved when the ratio of $CaCO_3$/red mud reached 1.5. The intermediate products of Ca_2FeAlO_5, i.e. $Ca_2Fe_2O_5$ and $CaFe_3O_5$, can also be seen. The content of $Ca_2Fe_2O_5$ firstly increased from 14.1% to 30.9% and then decreased to 9.0%, while the content of $CaFe_3O_5$ did not
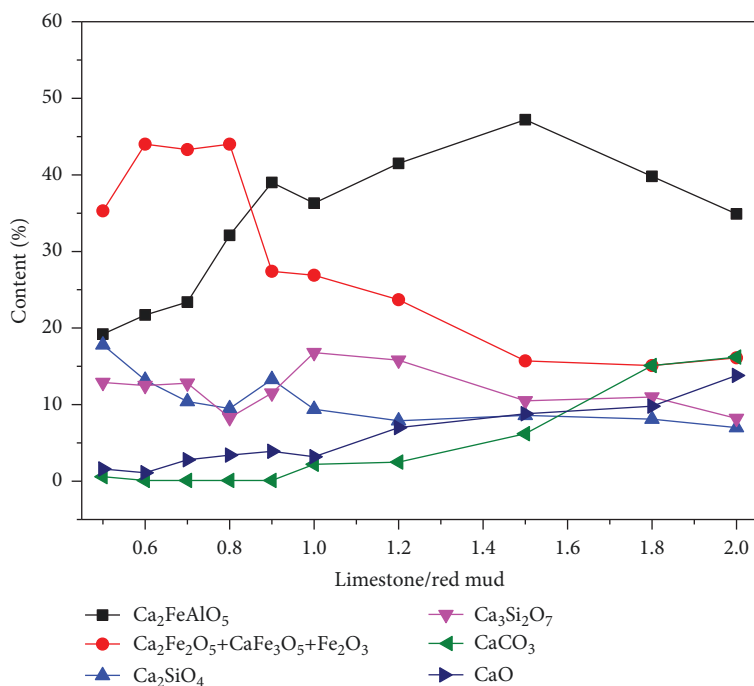
FIGURE 4: Variation in contents of major phases in NF at different $CaCO_3$/red mud ratios.

change much and remained at about 4%. In addition, the product containing Fe phase also had $Ca_3Fe_2(SiO_4)_3$; however, its content was minor (less than 4%).

As far as silicate products are concerned, three types of dicalcium silicates (abbreviated as C_2S), namely β, α, and α', were found in NF. Among these three types, β showed the highest content ranging from 5.2 to 14.0%, while the content of α and α' types was less than 6.1%. Since all three types of C_2S have hydration activity, therefore, a total amount of C_2S would be used for discussion. With the increase in the level of $CaCO_3$ raw materials, the total C_2S content decreased slightly. At a $CaCO_3$/red mud ratio of 1.5, the C_2S content was 8.1% while the total amount of the hydraulic contents (C_4AF+C_2S) was about 55%. The silicate also contained a certain amount of $Ca_3Si_2O_7$ (abbreviated as C_3S_2); however, it did not change much (range 8-16%) with the increase in the ratio of $CaCO_3$/red mud. It can also be seen from Figure 4 that at the 1.5 $CaCO_3$/red mud ratio, the content of C_3S_2 was found to be 10.5%. Although C_3S_2 does not have hydration activity, its volume expands in the carbonization environment [32], which can be beneficial to control the cracking and strength decrease caused by carbonization shrinkage.

The results (Figure 3 and Table 4) also show the presence of $CaCO_3$ residue and CaO (decomposition product of $CaCO_3$) in NF. Their content increased ($CaCO_3$: 0.1-16.2%; CaO: 1.1-13.8%) with the increase of the ratio of $CaCO_3$/red mud. At a $CaCO_3$/red mud ratio of 1.8 and higher, the content of $CaCO_3$ and CaO increased sharply, indicating that the effective use of raw materials was drastically reduced. At the 1.5 $CaCO_3$/red mud ratio, the $CaCO_3$ and CaO contents were found to be 6.2% and 8.8%, respectively. The contents of $NaAlSi_4$ and $Na_8Al_4Si_4O_{18}$, which are the residuals from red mud and having no hydration activity, were below 2%. Therefore, their influence on NF was negligible.

From the stoichiometric calculation of NF synthesis shown in Section 3.1.2, it can be seen that at the 1.5 $CaCO_3$/red mud ratio, the theoretical content of C_4AF in NF was 63.2%. However, the actual content of C_4AF in the synthesized NF was 47.2%, which was approximately 16% lower than the theoretical value. This is due to the reason that part of Fe in NF is in the form of $Ca_2Fe_2O_5$, $Ca_3Fe_2(SiO_4)_3$, and $CaFe_3O_5$ while the remaining unreacted part remained as Fe_2O_3. It should be mentioned here that the total amount of element Fe in Fe-related phases was 16.03%, which was close to the theoretical value of 14.55%, confirming the reliability of quantitative analysis. However, it is suggested that the conversion efficiency of raw materials to NF could be further improved by using the current experimental conditions. With regard to element Al, it was almost completely consumed to generate C_4AF. It is also noticed that the actual content of C_2S is 8.1%, which is quite different from the calculated value of 26.59%. The difference between the theoretical and experimental values is attributed to the formation of 10.5% $Ca_3Si_2O_7(C_3S_2)$ and 1.7% $Ca_3Fe_2(SiO_4)_3$, which in turn influenced Si-related phases. It is believed that Si-related phases in red mud were too stable to completely release SiO_2 required for the synthesis of NF.

In conclusion, at a $CaCO_3$/red mud ratio of 1.5, the content of C_2S+C_4AF in NF reached the maximum value. A further increase in $CaCO_3$ content in the raw materials resulted in the decrease of required C_4AF and unnecessary production of CaO and $CaCO_3$ residue. Hence, in the following sections, the ratio of $CaCO_3$/red mud would be taken as
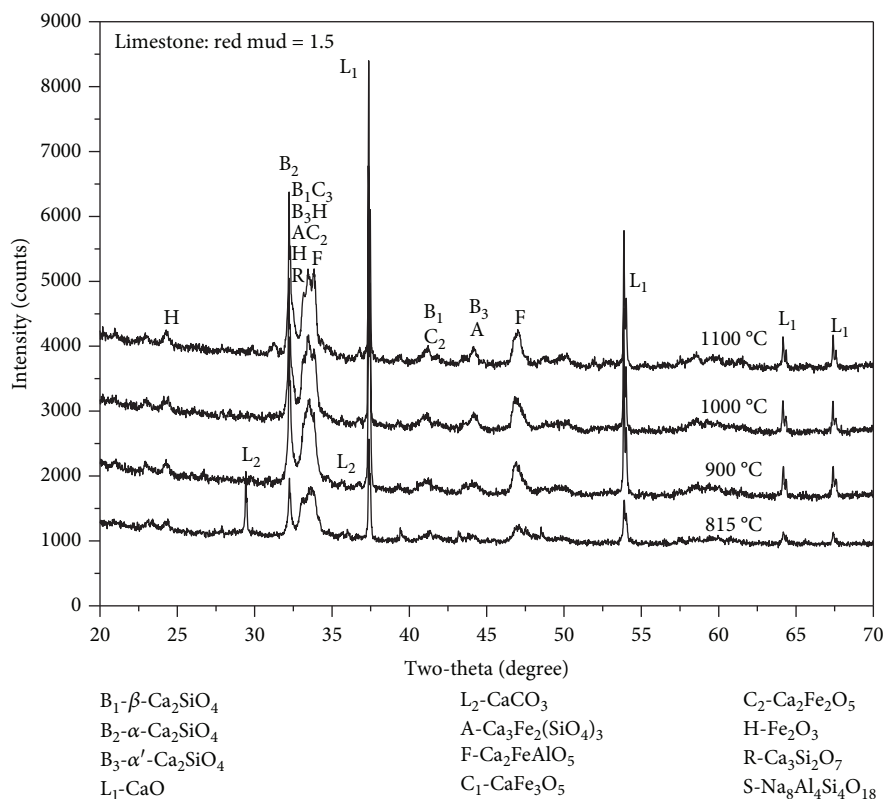
FIGURE 5: XRD spectra of NF produced at different heating temperatures.

1.5 and the heating temperature would be varied to evaluate the possibility of improving conversion efficiency of raw materials.

3.1.4. Influence of Heating Temperature. In order to study the effect of the heating temperature on NF prepared with a $CaCO_3$/red mud ratio of 1.5, the XRD of NF samples synthesized at 815, 900, 1000, and 1100°C, respectively, was evaluated. The results are presented in Figure 5. It can be seen that the peak intensity corresponding to brownmillerite (Ca_2FeAlO_5) increased slightly with the increase in temperature. However, above 900°C, the change was not significant. It is known that the synthesis temperatures of α-C_2S, α'-C_2S, and β-C_2S are higher than 1450, 725, and 500°C, respectively [33]. Therefore, the α-C_2S level increased sharply with the increase in temperature while α'-C_2S and β-C_2S were not influenced significantly by the increase in temperature.

In addition, it can be observed that above 900°C, the peak of $CaCO_3$ disappeared, while the peak of CaO gradually increased when the heating temperature was higher than 900°C, suggesting that extra heat was required to decompose $CaCO_3$ into CaO. The peak intensities of other products shown in Figure 5 remained unchanged. Therefore, it can be deduced that from the perspective of energy saving and efficiency, the temperature required to convert raw materials to target product (synthesis of NF) is 815°C.

3.1.5. Morphology and Fineness of NF. The morphology of typical NF synthesized at an optimal $CaCO_3$/red mud ratio

of 1.5 and heating temperature of 815°C is shown in Figure 6. It can be seen from Figure 6(a) that the sintered NF has a particle size of approximately 300 nm and its shape is nearly spherical. The comparison of BSE images of NF (Figure 6(b)) and PC (Figure 6(c)) for PC also shows that the size of the NF was much smaller than that of the PC particles.

3.2. Hydration of NF. After determining the optimal synthesis temperature of NF, SEM and XRD techniques were used to determine the hydration products of NF. The SE image after 28 days of NF hydration presented in Figure 7(a) shows that the morphology of the main hydration product is flaky. The BSE image of hydrated NF presented in Figure 7(b) shows that the prepared NF had been significantly hydrated at the age of 28 days. It suggests that the reduction of the particle size of ferrite to nanoscale could effectively accelerate hydration when compared with a traditional ferrite material, which has not shown significant hydration at the age of 28 days [34].

The XRD spectra of NF hydrated at the age of 3, 7, 14, 28, and 56 days are presented in Figure 8. At this time, a large number of early hydration products $C(A,F)H_{10}$ and a small amount of $C_2(A,F)H_8$ were formed. This confirmed that the prepared NF had hydrated significantly at 3 days. At this age, the content of C_2S in NF decreased and the content of hydration product $Ca(OH)_2$ increased, indicating that C_2S had also hydrated. However, during the first 56 days, the content of C_2S decreased slowly, which confirmed that the early hydration of C_2S was still slow. At

(a)

(b)

(c)
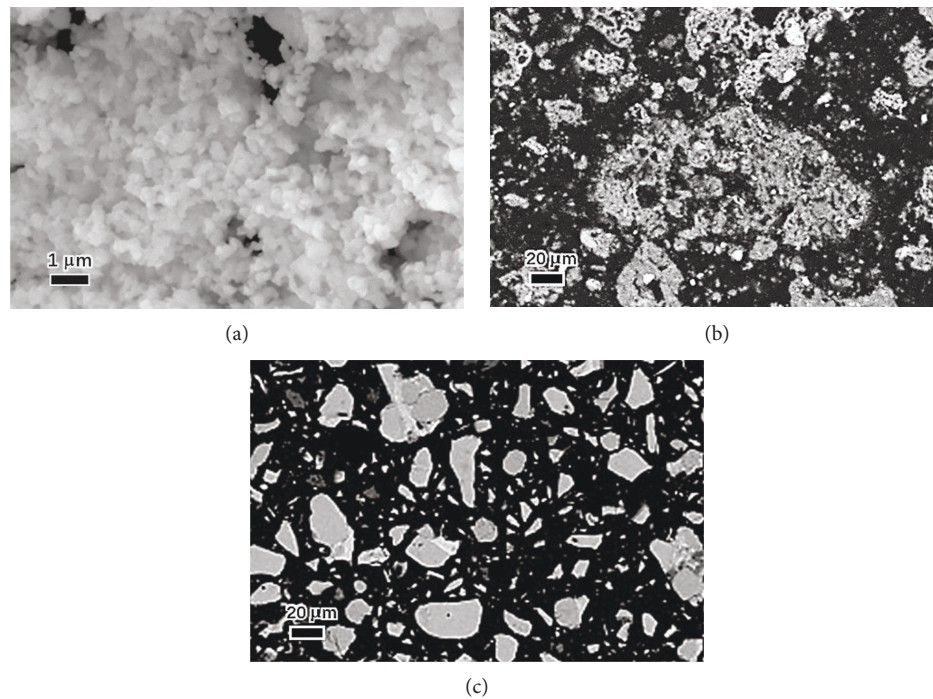
Figure 6: SEM images of NF produced at CaCO$_3$/red mud of 1.5 and temperature of 815°C. (a) NF (SE). (b) NF (BSE). (c) PC (BSE).
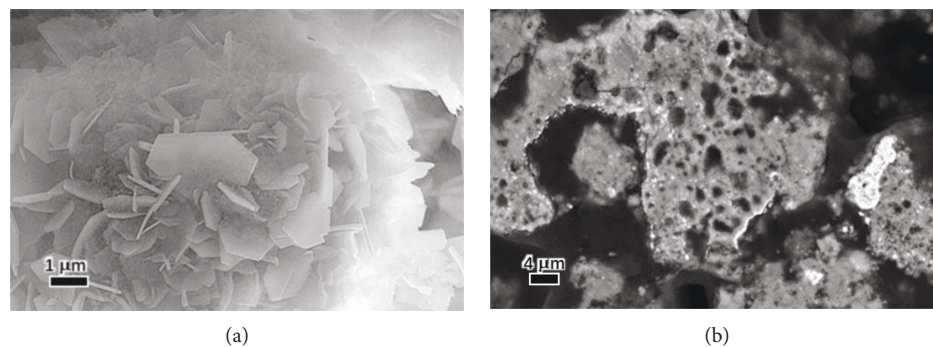

(a)

(b)

Figure 7: SEM images of hydrated NF at the age of 28 days. (a) Micrograph by SE. (b) Cross-sectional image by BSE.

the age of 7 days, the content of C(A,F)H$_{10}$ decreased and the content of C$_2$(A,F)H$_8$ increased due to the gradual transformation of C(A,F)H$_{10}$ to C$_2$(A,F)H$_8$ crystals. At 14 days, the content of C(A,F)H$_{10}$ decreased and the content of C$_2$(A,F)H$_8$ increased further. Meanwhile, C$_3$(A,F)H$_6$ started to appear [35]. At 28 days, the content of C$_3$(A,F)H$_6$ further increased while the contend of Ca(OH)$_2$ decreased. At this age, a diffraction peak of CaCO$_3$ appeared due to carbonation. At the age of 56 days, the C(A,F)H$_{10}$ crystal almost disappeared, C$_2$(A,F)H$_8$ content decreased significantly, and C$_3$(A,F)H$_6$ content increased significantly. This indicated that C(A,F)H$_{10}$ and C$_2$(A,F)H$_8$ were so unstable that they transformed into more stable C$_3$(A,F)H$_6$ at later ages and is consistent with the findings presented in references [15, 36].

3.3. Mechanical Properties of NF. In order to further investigate the properties of NF as an admixture, the mechanical

properties of cement mortars were determined by replacing a specific content of PC by 0, 5, 10, 15, and 20% of NF, respectively. The results of mechanical properties at the age of 3, 7, 14, and 28 days are presented in Figure 9. The figure indicates that the flexural and compressive strengths of all samples increased with the increase in the age of testing. As the replacement level of NF increased from 0% to 20%, the flexural and compressive strengths first increased and then decreased, reaching the maximum compressive and flexural strengths at 5% substitution level. Moreover, specimens prepared with 5% replacement level achieved the highest flexural and compressive strengths than the control mix (specimens with 0% replacement) at all ages. Compared with the control specimens, the flexural and compressive strengths of the 5% substitution specimens increased by 15.4% and 9.0%, respectively, at the age of 3 days, and by 9.0% and 6.7%, respectively, at 28 days. The increase in strength is much higher than that of mortar prepared with 5% traditional ferrite
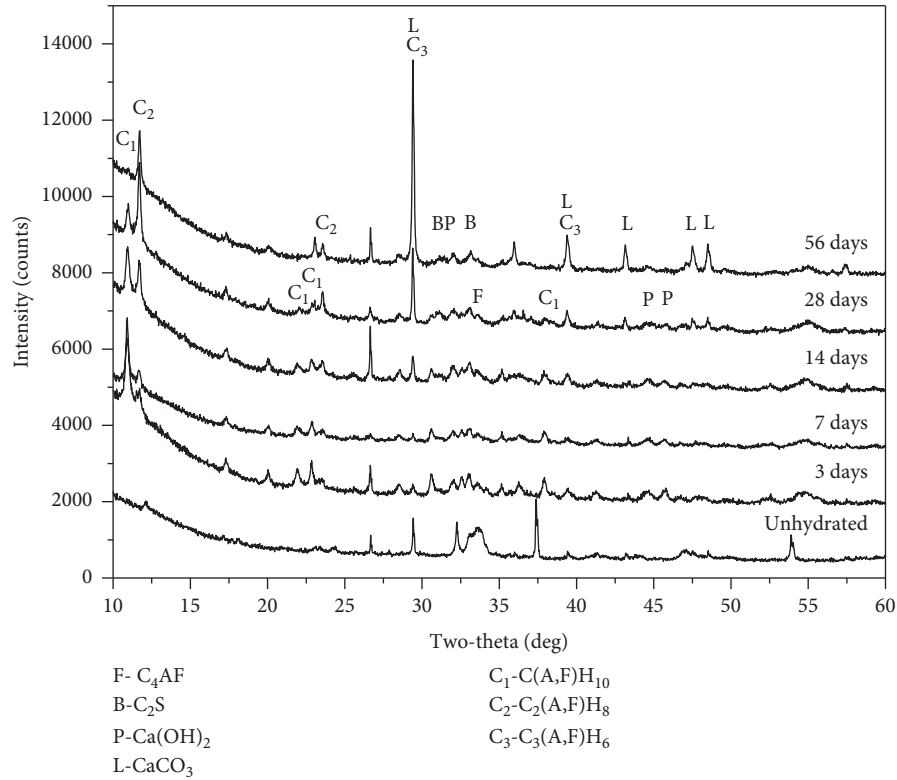
F- C_4AF

B-C_2S

P-Ca(OH)$_2$

L-CaCO$_3$

C_1-C(A,F)H$_{10}$

C_2-C$_2$(A,F)H$_8$

C_3-C$_3$(A,F)H$_6$

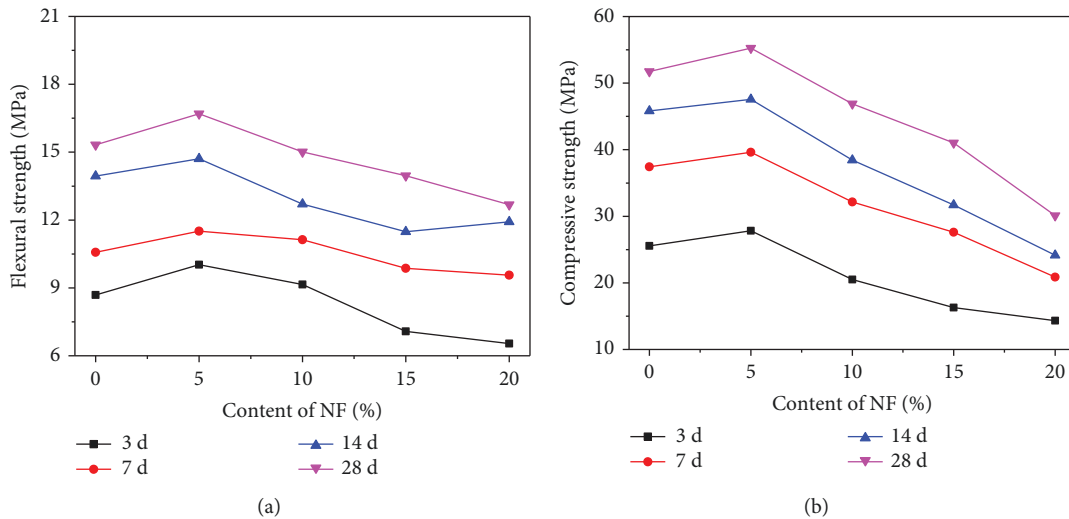FIGURE 8: XRD spectra of hydrated NF cured at different ages.

(a)

(b)

FIGURE 9: The flexural and compressive strength of cement mortars prepared with different contents of NF.

additive produced by red mud (compressive strength enhanced by 5% at 28 days) [37] as well as mortar prepared with 3.5% as-received red mud (compressive strength enhanced by 0% at 3 days and by 4.5% at 28 days) [38]. It indicates that reprocessing of red mud and nanocrystallization could effectively improve the mechanical properties on cementitious materials. Unfortunately, at other replacement levels, such as 10%, 15%, and 20%, the overall flexural strength and compressive strength were lower than control

specimens. Therefore, with increasing NF content in cement mortar, the mechanical properties of cement mortar did not always increase but achieved maximum mechanical strength at the 5% replacement level.

The increase in strength at 5% NF when compared with that of control specimen is believed to be due to the following reasons: (1) NF particles having nanoscale size were effective in filling and improving packing density of mortar, and this in turn reduced the porosity of the system. (2) The

appropriate amount of nanomaterials could improve the interfacial transition zone (ITZ) between sand and cement paste [39].

As mentioned earlier, when the dosage of NF exceeded 5%, the flexural and compressive strengths of mortar decreased. This can be attributed to the following reasons: (1) The hydration of C_2S and C_4AF in NF was still slower than that of PC, resulting in lower flexural and compressive strengths than the control mortar during the tested period (until 28 days). (2) It is believed that the NF particles might not have been sufficiently dispersed especially at high dosage and the aggregation of nanoparticles existed as defects in mortar and caused decrease in flexural and compressive strengths.

Therefore, the amount of NF dosage plays an important role in the strength development of cement mortar. Hence, higher compressive strength can be expected if the dispersion technique of NF in PC cement could be improved. However, further investigation is required and proposed for future research.

4. Conclusions

In this research, NF was synthesized by a chemical combustion method using red mud as one of the raw materials. By using stoichiometric calculation and experimental verification, the optimal conditions for NF preparation were found at a $CaCO_3$/red mud ratio of 1.5 and a heating temperature of 815°C. The synthesized NF particles were roughly spherical in shape with an approximate size of 300 nm. The dominant composition of NF was found to be C_4AF (47.2%) and C_2S (8.6%). The decrease in the particle size of ferrite enhanced early hydration. Flaky hydration products of $C(A,F)H_{10}$ and $C_2(A,F)H_8$ were formed and at later ages were gradually converted into a more stable cubic $C_3(A,F)H_6$. NF could enhance the mechanical properties when it was used as a replacement of cement in cement-based composite. At the 5% replacement level of cement with NF, the flexural and compressive strengths increased by 15% and 9%, respectively.

From the aspect of energy consumption and quality of product, NF was synthesized at a much lower temperature (≤1150°C) than traditional ferrite cement (1250-1300°C); thus, it would save a lot of sintering energy. The synthesized NF particles have a porous structure and are loosely agglomerated hence requiring slight grinding before it can be used as an admixture. This would greatly reduce the post grinding energy and further reduce the production cost. Additionally, the produced NF particles have a round shape with a relatively uniform particle size distribution, which is beneficial for the workability of concrete. In the future work, effort would be put to reduce the cost of fuels in order to reduce the overall production cost.

In general, red mud can be converted into hydraulic NF through a chemical combustion method and it provides a new approach for the utilization of red mud in construction industry.

Data Availability

The data used to support the findings of this study are included within the article.

Conflicts of Interest

The authors declare that there is no conflict of interest regarding the publication of this paper.

Acknowledgments

References

[1] S. Patel and B. K. Pal, "Current status of an industrial waste: red mud an overview," *Ijltemas*, vol. 4, no. 8, pp. 1–6, 2015.

[2] J. Ortega, M. Cabeza, A. Tenza-Abril, T. Real-Herraiz, M. Climent, and I. Sánchez, "Effects of red mud addition in the microstructure, durability and mechanical performance of cement mortars," *Applied Sciences*, vol. 9, no. 5, p. 984, 2019.

[3] V. Dethlefsen and H. Rosenthal, "Problems with dumping of red mud in shallow waters. A critical review of selected literature," *Aquaculture*, vol. 2, pp. 267–280, 1973.

[4] H. Zhang, H. Li, Y. Zhang, D. Wang, J. Harvey, and H. Wang, "Performance enhancement of porous asphalt pavement using red mud as alternative filler," *Construction and Building Materials*, vol. 160, pp. 707–713, 2018.

[5] S. Baseden and D. Grey, "Environmental study of the disposal of red mud waste," *Marine Pollution Bulletin*, vol. 7, no. 1, pp. 4–7, 1976.

[6] Y. Çengeloğlu, E. Kir, and M. Ersöz, "Recovery and concentration of Al(III), Fe(III), Ti(IV), and Na(I) from red mud," *Journal of Colloid and Interface Science*, vol. 244, no. 2, pp. 342–346, 2001.

[7] S. Sushil and V. S. Batra, "Catalytic applications of red mud, an aluminium industry waste: a review," *Applied Catalysis B: Environmental*, vol. 81, no. 1-2, pp. 64–77, 2008.

[8] J. Carneiro, D. M. Tobaldi, W. Hajjaji et al., "Red mud as a substitute coloring agent for the hematite pigment," *Ceramics International*, vol. 44, no. 4, pp. 4211–4219, 2018.

[9] C. Klauber, M. Gräfe, and G. Power, "Bauxite residue issues: II. Options for residue utilization," *Hydrometallurgy*, vol. 108, no. 1-2, pp. 11–32, 2011.

[10] C. Shi, P. E. Grattan-Bellew, and J. A. Stegemann, "Conversion of a waste mud into a pozzolanic material," *Construction and Building Materials*, vol. 13, no. 5, pp. 279–284, 1999.

[11] D. V. Ribeiro, J. A. Labrincha, and M. R. Morelli, "Potential use of natural red mud as pozzolan for Portland cement," *Materials Research*, vol. 14, no. 1, pp. 60–66, 2011.

[12] W. C. Tang, Z. Wang, Y. Liu, and H. Z. Cui, "Influence of red mud on fresh and hardened properties of self-compacting concrete," *Construction and Building Materials*, vol. 178, pp. 288–300, 2018.

[13] P. Krivenko, O. Kovalchuk, A. Pasko et al., "Development of alkali activated cements and concrete mixture design with high volumes of red mud," *Construction and Building Materials*, vol. 151, pp. 819–826, 2017.

[14] L. Zhang, M. Su, and Y. Wang, "The research and application of ferrite cement with high strength," *China Concrete And Cement Products*, no. 6, pp. 11–15, 1994.

[15] Y. Hong, "Preparation and properties of aluminoferrite cement clinker based on the slag of Ti-Si-V-Fe alloy-making from Titania-rich BF slag," in *Material Science*, p. 69, Wuhan University of Science and Technology, China National Knowledge Infrastructure, 2014.

[16] K. Behfarnia and N. Salemi, "The effects of nano-silica and nano-alumina on frost resistance of normal concrete," *Construction and Building Materials*, vol. 48, pp. 580–584, 2013.

[17] H. R. Jiang, Y. K. Zeng, M. C. Wu, W. Shyy, and T. S. Zhao, "A uniformly distributed bismuth nanoparticle-modified carbon cloth electrode for vanadium redox flow batteries," *Applied Energy*, vol. 240, pp. 226–235, 2019.

[18] H. Li, L. Luo, P. Kunal et al., "Oxygen reduction reaction on classically immiscible bimetallics: a case study of RhAu," *The Journal of Physical Chemistry C*, vol. 122, no. 5, pp. 2712–2716, 2018.

[19] H. Li, K. Shin, and G. Henkelman, "Effects of ensembles, ligand, and strain on adsorbate binding to alloy surfaces," *The Journal of Chemical Physics*, vol. 149, no. 17, article 174705, 2018.

[20] C. Duan, F. Li, M. Yang, H. Zhang, Y. Wu, and H. Xi, "Rapid synthesis of hierarchically structured multifunctional metal–organic zeolites with enhanced volatile organic compounds adsorption capacity," *Industrial & Engineering Chemistry Research*, vol. 57, no. 45, pp. 15385–15394, 2018.

[21] M. Katsioti, P. E. Tsakiridis, P. Giannatos, Z. Tsibouki, and J. Marinos, "Characterization of various cement grinding aids and their impact on grindability and cement performance," *Construction and Building Materials*, vol. 23, no. 5, pp. 1954–1959, 2009.

[22] L. Y. Li and G. K. Rutherford, "Effect of bauxite properties on the settling of red mud," *International Journal of Mineral Processing*, vol. 48, no. 3-4, pp. 169–182, 1996.

[23] P. F. Rossi, G. Caracciolo, and G. Busca, "Evolution of the surface of haematite prepared by thermal decomposition of goethite: a microcalorimetric study," *Colloids and Surfaces*, vol. 32, no. 1-2, pp. 75–85, 1988.

[24] S. Ananthakumar, G. Krishnapriya, A. D. Damodaran, and K. G. K. Warrier, "Thermal decomposition characteristics of boehmite gels under microwave heating and associated microstructural features," *Materials Letters*, vol. 35, no. 1–2, pp. 95–99, 1998.

[25] J. Felsche and S. Luger, "Phases and thermal decomposition characteristics of hydro-sodalites $Na_{6+x}[AlSiO_4]_6(OH)_x \cdot nH_2O$," *Thermochimica Acta*, vol. 118, no. 1, pp. 35–55, 1987.

[26] A. Tsetsekou, "A comparison study of tialite ceramics doped with various oxide materials and tialite–mullite composites: microstructural, thermal and mechanical properties," *Journal of the European Ceramic Society*, vol. 25, no. 4, pp. 335–348, 2005.

[27] J. Ye, W. Zhang, and D. Shi, "Effect of elevated temperature on the properties of geopolymer synthesized from calcined ore-dressing tailing of bauxite and ground-granulated blast furnace slag," *Construction and Building Materials*, vol. 69, no. 11, pp. 41–48, 2014.

[28] D. Herfort, G. K. Moir, V. Johansen, F. Sorrentino, and H. B. Arceo, "The chemistry of Portland cement clinker," *Advances in Cement Research*, vol. 22, no. 4, pp. 187–194, 2010.

[29] C. Wu and D. Liu, "Mineral phase and physical properties of red mud calcined at different temperatures," *Journal of Nanomaterials*, vol. 2012, Article ID 628592, 6 pages, 2012.

[30] H. Zhang, "Cement section 1:portland cement," in *Book of Building Materials in Civil Engineering*, pp. 46–423, Woodhead Publishing, Sawston, UK, 2011.

[31] M. Singh, S. N. Upadhayay, and P. M. Prasad, "Preparation of special cements from red mud," *Waste Management*, vol. 16, no. 8, pp. 665–670, 1996.

[32] J. Chang and H. Wu, "Study on carbonation mechanism of steel slag," *Journal of the Chinese Ceramic Society*, vol. 38, no. 7, pp. 1185–1190, 2010.

[33] W. Zhao and J. Chang, "Sol–gel synthesis and in vitro bioactivity of tricalcium silicate powders," *Materials Letters*, vol. 58, no. 19, pp. 2350–2353, 2004.

[34] Y. Guo, M. Su, J. Deng, and Y. Wng, "Study on hydration characteristics of iron phase in iron aluminate cement," *China Academic Journal Electronic Publishing House*, vol. 17, no. 4, pp. 296–301, 1989.

[35] B. Dou, "Sythesis and research on properties of nano-cement clinker minerals," in *Material Engineering*, p. 56, Hebei United University, China National Knowledge Infrastructure, 2014.

[36] C. Gosselin, "Microstructural development of calcium aluminate cement based systems with and without supplementary cementitious materials," in *Institute of Materials*, p. 234, EPFL, Lausanne, Switzerland, 2009.

[37] I. Vangelatos, G. N. Angelopoulos, and D. Boufounos, "Utilization of ferroalumina as raw material in the production of Ordinary Portland Cement," *Journal of Hazardous Materials*, vol. 168, no. 1, pp. 473–478, 2009.

[38] P. E. Tsakiridis, S. Agatzini-Leonardou, and P. Oustadakis, "Red mud addition in the raw meal for the production of Portland cement clinker," *Journal of Hazardous Materials*, vol. 116, no. 1-2, pp. 103–110, 2004.

[39] H. Li, H. Xiao, J. Yuan, and J. Ou, "Microstructure of cement mortar with nano-particles," *Composites Part B: Engineering*, vol. 35, no. 2, pp. 185–189, 2004.